International Journal of Nanomedicine

Dovepress
open access to scientific and medical research

Open Access Full Text Article

ORIGINAL RESEARCH

ICG-Loaded PEGylated BSA-Silver Nanoparticles for Effective Photothermal Cancer Therapy

This article was published in the following Dove Press journal:
International Journal of Nanomedicine

Taehoon Park[1,*]
Sumi Lee[2,*]
Reeju Amatya[1]
Heesun Cheong[3]
Cheol Moon[4]
Hyun Duck Kwak[5]
Kyoung Ah Min[2]
Meong Cheol Shin[1]

[1]College of Pharmacy and Research Institute of Pharmaceutical Sciences, Gyeongsang National University, Jinju, Gyeongnam 52828, Republic of Korea; [2]College of Pharmacy and Inje Institute of Pharmaceutical Sciences and Research, Inje University, Gimhae, Gyeongnam 50834, Republic of Korea; [3]Division of Cancer Biology, National Cancer Center, Goyang, Gyeonggi-do 10408, Republic of Korea; [4]College of Pharmacy, Sunchon National University, Suncheon, Jeonnam 57922, Republic of Korea; [5]Department of Ophthalmology, Busan Paik Hospital, Inje University College of Medicine, Busanjin-gu, Busan 47392, Republic of Korea

*These authors contributed equally to this work

Purpose: Indocyanine green (ICG), a near infrared (NIR) dye clinically approved in medical diagnostics, possesses great heat conversion efficiency, which renders itself as an effective photosensitizer for photothermal therapy (PTT) of cancer. However, there remain bottleneck challenges for use in PTT, which are the poor photo and plasma stability of ICG. To address these problems, in this research, ICG-loaded silver nanoparticles were prepared and evaluated for the applicability as an effective agent for photothermal cancer therapy.

Methods and Results: PEGylated bovine serum albumin (BSA)-coated silver core/shell nanoparticles were synthesized with a high loading of ICG ("PEG-BSA-AgNP/ICG"). Physical characterization was carried out using size analyzer, transmission electron microscopy, and Fourier transform infrared spectrophotometry to identify successful preparation and size stability. ICG-loading content and the photothermal conversion efficiency of the particles were confirmed with inductively coupled plasma mass spectrometry and laser instruments. In vitro studies showed that the PEG-BSA-AgNP/ICG could provide great photostability for ICG, and their applicability for PTT was verified from the cellular study results. Furthermore, when the PEG-BSA-AgNP/ICG were tested in vivo, study results exhibited that ICG could stably remain in the blood circulation for a markedly long period (plasma half-life: 112 min), and about 1.7% ID/g tissue could be accumulated in the tumor tissue at 4 h post-injection. Such nanoparticle accumulation in the tumor enabled tumor surface temperature to be risen to 50°C (required for photo-ablation) by laser irradiation and led to successful inhibition of tumor growth in the B16F10 s.c. syngeneic nude mice model, with minimal systemic toxicity.

Conclusion: Our findings demonstrated that PEG-BSA-AgNPs could serve as effective carriers for delivering ICG to the tumor tissue with great stability and safety.

Keywords: silver nanoparticle, bovine serum albumin, indocyanine green, photothermal therapy, cancer

Correspondence: Kyoung Ah Min
College of Pharmacy and Inje Institute of Pharmaceutical Sciences and Research, Inje University, Gimhae, Gyeongnam 50834, Republic of Korea
Tel +82 55 320 3459
Fax +82 55 320 3940
Email minkahh@inje.ac.kr

Meong Cheol Shin
College of Pharmacy and Research Institute of Pharmaceutical Sciences, Gyeongsang National University, Jinju, Gyeongnam 52828, Republic of Korea
Tel +82 55 772 2421
Fax +82 55 772 2429
Email shinmc@gnu.ac.kr

Introduction

Photothermal therapy (PTT) is a minimally invasive mode of treatment that mainly relies on photosensitizers that possess the ability to absorb light and convert it into heat with laser irradiation.[1,2] The induced hyperthermia could cause cancer cell death by evoking various events such as cell lysis and protein denaturation or aggregation.[2–5] Recent studies suggested that hyperthermia may also enhance the therapeutic efficacy of chemotherapy and radiotherapy.[6–8] Hence, to date, enormous attention has been paid to the development of strategies for effective PTT.[9–12]

ICG is a clinically approved fluorescent dye used as an indicator of various medical conditions.[13,14] Apart from its functionality as a dye, the ICG can also

convert light-to-heat as well as produce free radicals by light activation.[15] Owing to these properties, ICG has great potentials to serve as an effective photosensitizer for PTT-based treatment of cancer. Nevertheless, there remains a bottleneck challenge to address for its successful use in the clinics. It is the poor photo and plasma stability of the ICG. The ICG is highly vulnerable to decomposition by laser irradiation.[16] Furthermore, when administered intravenously, the ICG possesses a very short plasma half-life (3–4 min); rapidly being excreted via the liver and bile ducts after metabolism.[17] Therefore, various approaches have been attempted to stabilize the ICG, which includes loading the ICG into nanoparticles. In many previous reports, nanoparticle encapsulation of the ICG showed enhancement of both the photostability and the plasma stability.[18–21] Despite the successful reports, there are yet unresolved issues to be addressed to make a more ideal ICG-loaded nanoparticulate system. Some of the remaining issues include 1) avoiding substantial quenching of ICG by complexation with the nanomaterials that have been observed from mixing with reduced graphene oxides, gold, and iron oxides, etc., 2) need of more simple and mild synthesis conditions that could work at low reaction temperature (likely 4°C), 3) ensuring stable and high loading of ICG, and 4) securing sufficient blood circulation time for high tumor accumulation of the ICG after systemic administration.

Silver nanoparticles (AgNPs), mainly synthesized by reduction of silver ions, possesses anti-cancer activity.[22,23] The main mechanism for the cytotoxicity is yet to be resolved, but it is postulated to be related to the cell membrane damage caused by the silver nanoparticles itself or silver ions released from the particles.[24] The cytotoxic activities of the silver nanoparticles are, however, available only at high concentrations (several hundred micromolar concentrations). In this regard, loading anti-cancer drugs or photosensitizers such as ICG to silver nanoparticles could be a highly effective way to improve their utility for the treatment of cancer.[25] Moreover, as a nanocarrier, the silver nanoparticles could be highly favorable specifically for heat-labile and water-soluble ICG. This is because the synthesis process of the silver nanoparticles does not require either organic solvents or heating.[24]

In this research, we developed ICG-loaded PEGylated BSA silver nanoparticles (PEG-BSA-AgNP/ICG) (Figure 1). After preparation, the physicochemical properties of the prepared nanoparticles were examined by transmission electron microscopy (TEM), UV-VIS spectrum analysis, dynamic light scattering (DLS) and Fourier transform infrared (FT-IR) spectrophotometry. The applicability of PEG-BSA-AgNP/ICG for photothermal cancer therapy was then explored in vitro and in vivo. The findings of this study suggested that PEG-BSA-AgNP/ICG could serve as an effective agent for photothermal cancer therapy.

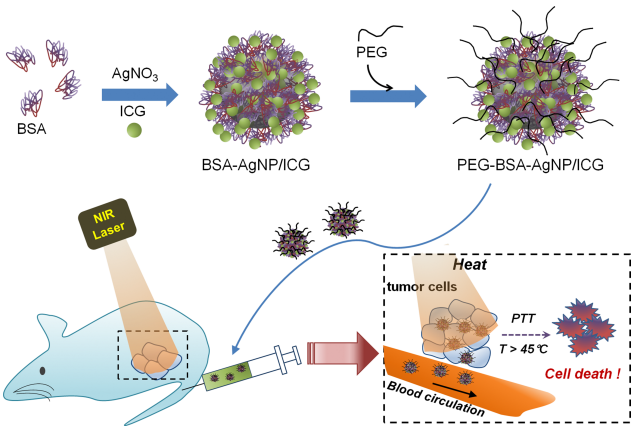

Figure 1 Scheme of the PEG-BSA-AgNP/ICG-based photothermal cancer therapy. The encapsulation of indocyanine green (ICG) in PEGylated BSA-coated silver nanoparticles could provide an enhanced photo and plasma stability for ICG, leading to successful inhibition of tumor growth with local laser irradiation to the tumor site.
Abbreviations: PEG, polyethylene glycol; BSA, bovine serum albumin; AgNPs, silver nanoparticles; NIR, near infrared; PTT, photothermal therapy.

Materials and Methods

Materials

BSA was purchased from Amresco (Solon, OH, USA). Silver nitrate ($AgNO_3$) solution, Sodium borohydride ($NaBH_4$) were purchased from Sigma Aldrich (St. Louis. MO, USA) Polyethylene glycol (NHS-PEG; 5 kDa) was purchased from JenKem USA (Allen, TX, USA). ICG was purchased from TCI (Tokyo, Japan).

Synthesis of PEG-BSA-AgNP/ICG

BSA solution was prepared by dissolving 100 mg of BSA in 1 mL of double-distilled water (DDW). To 29 mL of DDW, the as-prepared BSA solution and 1 mg of $NaBH_4$ was added. After then, 0.4 mL of 10 mM $AgNO_3$ solution was mixed with 4 mL of 1 mg/mL ICG, and the mixture was dropwisely added to the BSA/$NaBH_4$ solution using a syringe (30-gauge needle) while stirring at 1000 rpm at 4°C. The colorless solution became brownish-green, indicating the formation of silver nanoparticles. The $NaBH_4$ and non-encapsulated ICG were removed by using an ultracentrifugal device (membrane cut-off: 100 kDa). Next, the PEGylation was carried out by mixing the prepared BSA-AgNP/ICG with 30 mg of NHS-PEG (5 kDa), and

incubation for 2 h at 4°C. The unreacted PEG was removed by centrifugation of the particle solution by using the ultracentrifugal device (membrane cut-off: 100 kDa). Specifically, for the PEG-BSA-AgNP/ICG used in animal studies, the final samples were prepared in phosphate buffer saline (PBS; pH 7.4 with 0.15 M NaCl), while, for the rest of the studies, in DDW.

Physical Characterization of PEG-BSA-AgNP/ICG

The morphology of the prepared PEG-BSA-AgNP/ICG was examined by TEM (Tecnai 12, FEI, Hillsboro, Oregon, USA). To verify the synthesis of silver nanoparticles and ICG loading to the particles, the absorption spectrum of PEG-BSA-AgNP /ICG was detected in the range of 300–900 nm by using a Synergy H1 Hybrid Multi-Mode Reader (BioTek US, Winooski, VT, USA). In addition, FT-IR spectrophotometry was carried out (at the wavelength range of 400–4000 cm^{-1}) to prove the presence of BSA and PEG in the particles by using an FT-IR microscope (VERTEX 80v, Bruker, Billerica, MA, USA). Quantification of BSA, silver, PEG, and ICG was by BCA protein assay, inductively coupled plasma mass spectrometry (ICP-MS), barium iodide assay[26] and UV-VIS spectrophotometry, respectively. The hydrodynamic size distribution and size stability of the particles were determined by DLS using a light scattering spectrometer (Zetasizer Nano ZS, Malvern Panalytical Ltd, Malvern, United Kingdom).

Determination of the Photothermal Activity of PEG-BSA-AgNP/ICG

To examine the photothermal activity of PEG-BSA-AgNP /ICG induced by NIR light, free ICG and PEG-BSA-AgNP /ICG samples were prepared at varying concentrations (0, 5, 10, 20 or 30 μg/mL for free ICG and, for PEG-BSA-AgNP /ICG, 0, 5, 10, 20, 30 or 50 μg/mL as ICG) in Eppendorf tubes. Both the ICG and PEG-BSA-AgNP/ICG samples were irradiated with laser (885 nm, 1.3 W, spot size: 5 × 8 mm^2, MDL-III-885, Changchun New Industries Optoelectronics Tech Co. Ltd, Changchun, China) for 20 min, and the temperature of the samples was monitored using an infrared camera (FLIR Systems, E5, Boston, MA, USA). In addition, to evaluate the thermal stability, the free ICG, PEG-BSA-ICG mixture, and PEG-BSA-AgNP/ICG samples were irradiated with a laser at 1.3 W for 3 repeating cycles of switch "on and off". The PEG-BSA-ICG mixture was prepared by mixing PEG-BSA with ICG at about 1:4 molar ratio (the same molar ratio that was achieved from the PEG-BSA-AgNP/ICG).

Cell Culture

B16F10 murine melanoma cell line was purchased from the Korean cell line bank (KCLB, Seoul, Republic of Korea). The B16F10 cells were cultured in complete DMEM medium containing 10% FBS, 1% antibiotic antimycotic and 1% penicillin-streptomycin, and the culture was maintained in a humidified incubator (5% CO_2) at 37ºC.

Cellular Analyses for Anti-Cancer Activity

B16F10 cells were seeded onto 96-well plates (5×10^3 cells/well) and incubated overnight. The cells were then treated with varying concentrations of PEG-BSA-AgNP /ICG (10^{-8} – 10^{-2} M as Ag). After incubation for 48 h, the relative cell viability was determined by using WST-1 assay, according to the vendor's protocol (iNtRON Biotechnology, Daejeon, Republic of Korea). To evaluate the photothermal cytotoxic effects by PEG-BSA-AgNP /ICG, B16F10 cells seeded on 96-well plates (5×10^3 cells/well) were treated with PEG-BSA-AgNP/ICG (30 μM as Ag) and laser was irradiated for 20 min with different laser outputs that could provide maximum medium temperatures of 40, 45 and 50°C, respectively.

Animal Studies

Animal experiments were carried out in accordance with the National Institute of Health Guidelines on the Use of Laboratory Animals and the protocol approved by the university's committee for animal research of Gyeongsang National University (GNU-180,724-M0037).

Pharmacokinetics (PK)

Ten healthy ICR mice (6 weeks old; Hana Co. Ltd, Busan, Republic of Korea) were divided randomly into two groups. The mice were administered with either BSA-Ag /ICG or PEG-BSA-Ag/ICG via tail vein injection at doses of 12 mg/kg as ICG. After then, blood was collected at pre-determined time points (0, 0.5, 1, 2, 4 and 6 h post-administration), and plasma samples were obtained by centrifugation of the blood at 3000 rpm for 3 min. The ICG in the plasma samples was quantified by measurement of absorbance at 790 nm.

Tissue Distribution and Liver Toxicity

B16F10 cells (10^7 cells/mouse) were injected (s.c.) into the right flank of 5 athymic nude mice (6 weeks old; Hana

Co. Ltd), and the tumor size was measured with a vernier caliper every day. The tumor size (V) was estimated by using the formula of V (mm^3) = ($a^2 \times b$)/2, where V is the volume, a is the width and b is the length of tumor. When the average tumor size reached 300 mm^3, B16F10 s.c. syngeneic tumor-bearing mice were administered with PEG-BSA-AgNP/ICG (12 mg/kg as ICG) via tail vein injection. At 4 h post-administration, the mice were euthanized and the major organs (kidney, tumor, lung, spleen, heart, and liver) were harvested. The fluorescent images of the mice organs were acquired by using FOBI Fluorescence In Vivo Imaging System (NeoScience Co., Ltd., Seoul, Republic of Korea) using an NIR channel. The images were analyzed using NEOimage software (NeoScience Co., Ltd.). The ICG contents in the tissues were quantified by measuring the absorbance at 790 nm after the homogenization of tissues. In a separate study, ICR mice (N = 3) were administered with either PBS or PEG-BSA-AgNP/ICG (12 mg/kg as ICG) via tail vein injection. The urine samples were collected up to 12 h and the serum samples were at 12 h post-administration. After euthanizing the mice, the liver and kidney were harvested. The liver, kidney, and urine samples were digested with nitric acid (HNO_3) and the silver contents were quantified by inductively coupled plasma-optical emission spectroscopy (ICP-OES). Also, the collected serum samples were submitted to the Southeast Medi-Chem Institute (Pusan, Republic of Korea) for liver function (AST & ALT) analysis.

In vivo Evaluation of the Photothermal Activity of PEG-BSA-AgNP/ICG

When the average tumor size reached 300 mm^3, B16F10 tumor-bearing nude mice (N = 5) were administered with PEG-BSA-AgNP/ICG (12 mg/kg as ICG) via the tail vein. At 4 h post-administration, the mice were anesthetized with ketamine/xylazine mixture, and then the tumors were irradiated for 20 min with a diode laser (λ = 885 nm) at varying laser output (0.5–0.95 W). The highest temperature of the tumor surface was monitored using an infrared camera (E5, FLIR Systems).

Tumor Growth Inhibition

Four days after tumor implantation (at day 4) when the average tumor sizes reached 100 mm^3, B16F10 s.c. syngeneic tumor-bearing mice were divided into 4 groups (N = 5). Groups 1 and 2 were administered with PBS, while groups 3 and 4 were administered with PEG-BSA-AgNP/ICG (12 mg/kg as ICG) via tail vein injection. For groups 2 and 4, at 4 h post-administration, the mice were anesthetized with i.p. injection of ketamine/xylazine mixture and the tumor regions were irradiated for 20 min with a diode laser (λ = 885 nm) at a laser output of 0.9 W. Tumor size and bodyweight of the treated mice were monitored daily. The study was continued until the average tumor size of the PBS control mice (group 1) reached 1000 mm^3.

Histological Analysis

After the efficacy study was terminated, the mice were sacrificed and the major organs including tumor, kidney, liver, lung, spleen, and heart were harvested and fixed in 10% formalin. The tissue samples were dissected (8 μm thick) and then embedded in paraffin. The paraffin sections were used for the staining with hematoxylin and eosin (H&E) reagents to assess any tissue toxicity. As reported previously,[27] after the staining with hematoxylin solution, the slides were serially washed with absolute ethanol and then 95% ethanol. The slides were counterstained by the eosin solution and then washed with water, 8095% ethanol, absolute ethanol and xylene.

Statistical Analysis

All data are presented as mean ± standard deviation (SD). The statistical significance was analyzed by 1-way ANOVA and Tukey's multiple comparison test as the post hoc test. Any result yielding a p-value of less than 0.05 was considered statistically significant.

Results

Synthesis and Characterization of PEG-BSA-AgNP/ICG

The preparation of PEG-BSA-AgNP/ICG was carried out in two steps. First, BSA-AgNP/ICG was synthesized by reducing Ag^+ with $NaBH_4$ in the presence of BSA. After removal of the unloaded ICG, in the next step, PEGylation was carried out by conjugation of PEG-NHS (5 kDa) to the amine groups of the BSA coating via adopting the NHS chemistry (Figure 1). The successful preparation of PEG-BSA-AgNP/ICG was characterized in detail. First, as shown in Figures 2A and 2B, the formation of silver nanoparticles and their morphology were identified through TEM imaging. The PEG-BSA-AgNP/ICG was observed as globular but irregular shaped nanoparticles

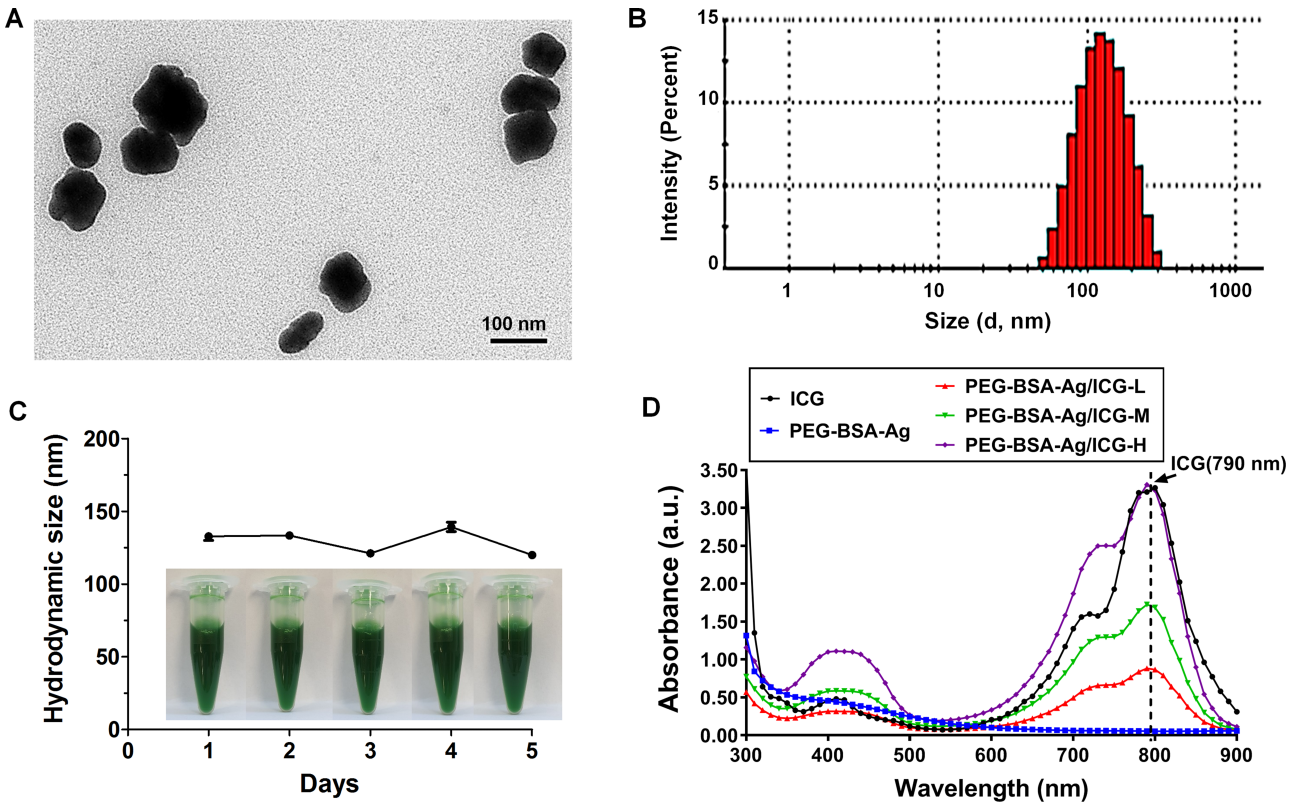

Figure 2 Physical characterization of the PEG-BSA-AgNP/ICG. (**A**) Representative transmission electron microscopic images of the PEG-BSA-AgNP/ICG. (**B**) The mean hydrodynamic size of PEG-BSA-AgNP/ICG by dynamic light scattering. (**C**) Size stability of the PEG-BSA-AgNP/ICG. (**D**) UV/VIS spectrophotometry of PEG-BSA-AgNP/ICG.
Abbreviations: PEG, polyethylene glycol; BSA, bovine serum albumin; AgNPs, silver nanoparticles; ICG, indocyanine green; PEG-BSA-AgNP/ICG, ICG-loaded PEGylated BSA-coated silver nanoparticles; UV/VIS, ultraviolet/visible; L, M and H refers to low, medium, and high concentration.

with average diameters of about 100 nm. The mean hydrodynamic size of the PEG-BSA-AgNP/ICG determined by DLS was 131.5 (±2.7) nm (PDI: 0.25) (Figure 2B), and the average zeta potential was −34.8 (±0.6) mV. As shown in Figure 2C, the size of PEG-BSA-AgNP/ICG was stably maintained during 5 days after synthesis without any sign of aggregation. The formation of silver nanoparticles was further evidenced by the UV-VIS spectrum (Figure 2D); as the peak at 420 nm, a characteristic surface plasmon resonance band of silver nanoparticles, was observed from all the nanoparticle samples.[28] The successful loading of ICG to the BSA-Ag nanoparticles was also confirmed by UV-VIS spectrophotometry (Figure 2D). The absorption peak at 790 nm distinct for ICG was observed from all the PEG-BSA-Ag/ICG samples prepared at high, medium and low concentration.[29] Finally, the presence of BSA coating on the nanoparticle surface and PEGylation was verified by FT-IR. As shown in Figure 3, the FT-IR spectra of PEG-BSA-AgNP/ICG displayed several characteristic peaks. The peak at 613 cm^{-1} was attributed to the lysine residues in BSA; indicating that BSA is incorporated into the PEG-BSA-AgNP/ICG.[30] Furthermore, the characteristic peak at 1100 cm^{-1} of PEG, assigned to the stretching vibration of -C–O-C-, was also clearly observed from the free PEG and PEG-BSA-AgNP/ICG, but not from the BSA-AgNP/ICG.[31] Overall, all these results confirmed the successful preparation of the PEG-BSA-AgNP/ICG. With the established recipe, based on the quantification results, the final composition of the PEG-BSA-Ag/ICG was: PEG 4.5 mg, BSA 64 mg, Ag 220 μg, and ICG 3.1 mg (4.8% loading against BSA, and 77.5% loading efficiency).

In vitro Photothermal Activity of PEG-BSA-AgNP/ICG

The photothermal activity and photostability of free ICG and PEG-BSA-AgNP/ICG were assessed in vitro, and the data are summarized in Figure 4. With laser irradiation, the temperature of free ICG solutions initially exhibited a rapid rise but, after reaching the highest at around 4 min, gradually decreased to the control level (Figure 4A). Higher temperature was achieved with increasing concentration of the ICG

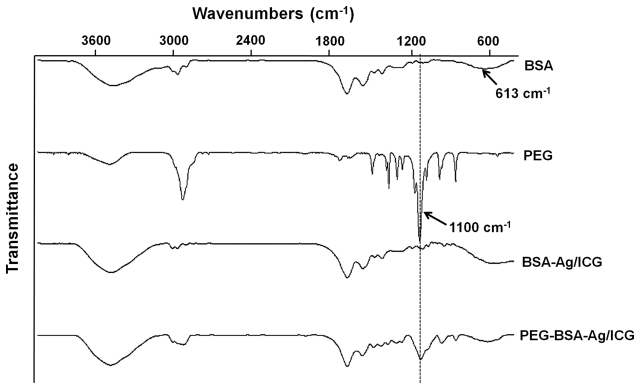

Figure 3 FT-IR data for the PEG-BSA-AgNP/ICG. The PEG-BSA-AgNP/ICG spectrum showed the characteristics peaks of BSA and PEG. The peaks at 613 and 1100 cm^{-1} were attributed to the lysine residues in BSA and the stretching vibration of "-C–O-C-" in the PEG.

Abbreviations: FT-IR, Fourier-transform infrared spectroscopy; PEG, polyethylene glycol; BSA, bovine serum albumin; AgNPs, silver nanoparticles; ICG, indocyanine green; PEG-BSA-AgNP/ICG, ICG-loaded PEGylated BSA-coated silver nanoparticles.

(from 41°C at 5 μg/mL ICG to 58.8°C at 30 μg/mL of ICG). Similar to the free ICG, concentration-dependent temperature rise was also observed from PEG-BSA-AgNP/ICG dispersions with laser irradiation (Figure 4B). The maximum temperatures observed from PEG-BSA-AgNP/ICG dispersions were slightly lower (41.3°C vs 44.9°C and 54.8°C vs 58.8°C at 10 and 30 μg/mL of ICG, respectively) than those of free ICG solutions when compared at the same concentrations. However, unlike the free ICG, the temperature of PEG-BSA-AgNP/ICG samples reached a plateau after the initial rise and well-maintained the highest temperature during the 20 min of laser irradiation. The maximum temperatures were linearly correlated to the ICG concentrations of the PEG-BSA-AgNP/ICG samples. As shown in Figure 4C, when free ICG, PEG-BSA-ICG mixture and PEG-BSA-AgNP/ICG were irradiated with a laser by using switch "on-and-off" mode, the maximum temperatures observed from the free ICG solution and the PEG-BSA-ICG mixture were markedly decreased after each cycle. However, in sharp contrast, the PEG-BSA-AgNP/ICG dispersion showed nearly the same temperature-vs-time profile for each cycle; evidencing superior photostability of the ICG encapsulated in the silver nanoparticles. Consistently, when the UV-VIS spectra of the free ICG, PEG-BSA-ICG mixture, and the PEG-BSA-AgNP/ICG were obtained before and after 20 min of laser

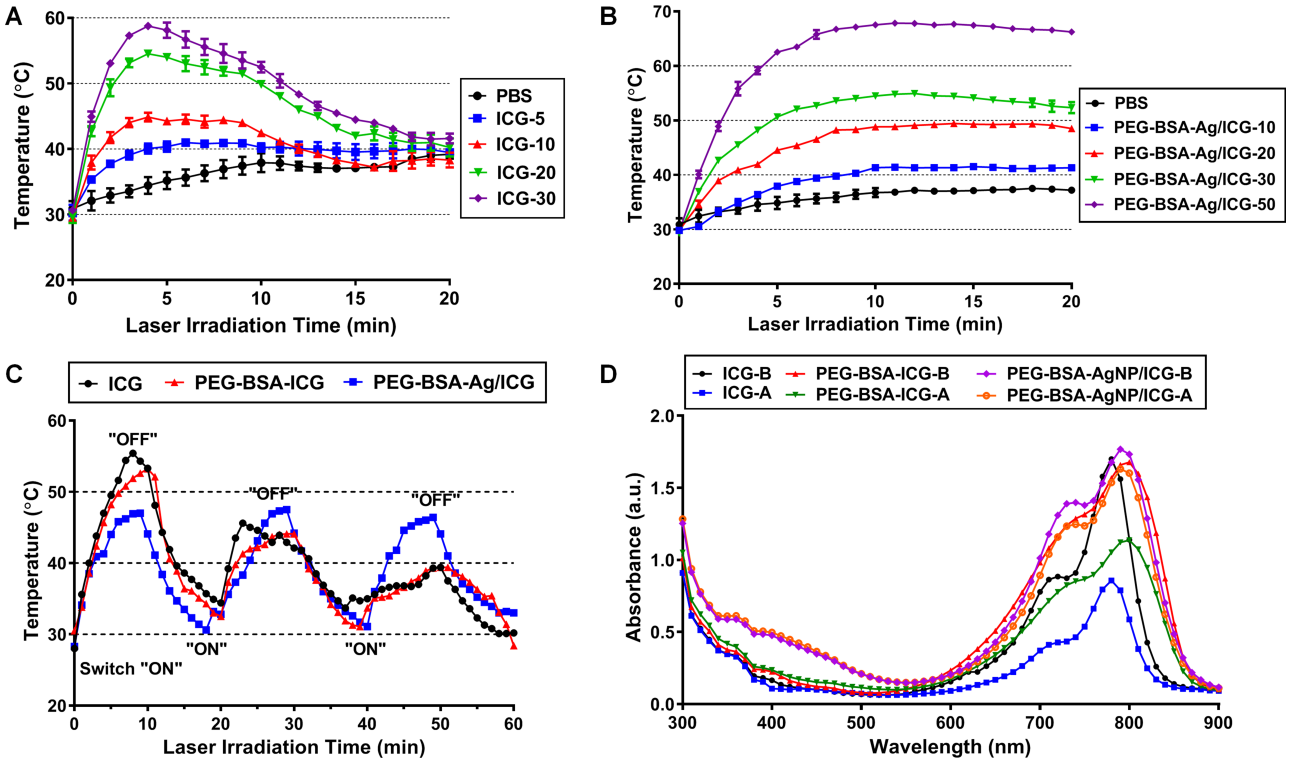

Figure 4 In vitro evaluation of the photothermal activity of the PEG-BSA-AgNP/ICG. (**A**) Temperature-versus-time profiles of the free ICG solution (at 5–30 μg/mL) after laser irradiation at 1.3 W. (**B**) Temperature-versus-time profiles of the PEG-BSA-AgNP/ICG dispersion (at 10–50 μg/mL as ICG) after laser irradiation at 1.3 W. (**C**) Temperature-versus-time profiles of free ICG, PEG-BSA-ICG mixture, and PEG-BSA-AgNP/ICG dispersion by laser irradiation at 1.3 W for three repeating cycles of a switch "on and off" mode. (**D**) UV-VIS spectra of ICG, PEG-BSA-ICG, and PEG-BSA-AgNP/ICG, before and after laser irradiation for 20 min.

Abbreviations: PEG, polyethylene glycol; BSA, bovine serum albumin; AgNPs, silver nanoparticles; ICG, indocyanine green; PEG-BSA-ICG, a mixture of PEG-BSA and ICG; PEG-BSA-AgNP/ICG, ICG-loaded PEGylated BSA-coated silver nanoparticles; UV/VIS, ultraviolet/visible; NIR, near infrared; PBS, phosphate buffer saline; PTT, photothermal therapy.

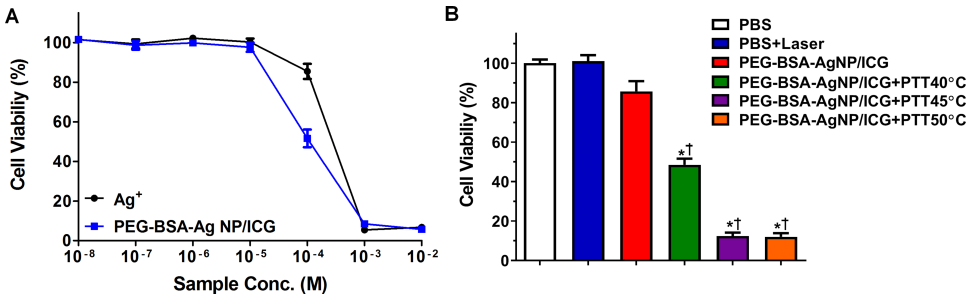

Figure 5 Cellular analysis of the anti-tumor activity of PEG-BSA-AgNP/ICG-based photothermal therapy. (**A**) Anti-tumor activity of Ag^+ and PEG-BSA-AgNP/ICG on B16F10 cells. The B16F10 cells were treated with varying concentrations of either Ag^+ or PEG-BSA-AgNP/ICG (10^{-8} – 10^{-2} M as Ag) and then, after 48 h incubation, the relative cell viability was determined using WST-1 assay. (**B**) Cytotoxicity of PEG-BSA-AgNP/ICG on B16F10 cells with photothermal treatment (PTT) at maximum medium temperatures of 40, 45, or 50°C. The statistically significant differences in the cytotoxicity levels were compared by 1-way ANOVA and post hoc Tukey's multiple comparison test. *$P < 0.05$ vs PBS control, †$P < 0.05$ vs PEG-BSA-AgNP/ICG-treated cells without laser irradiation.
Abbreviations: PEG, polyethylene glycol; BSA, bovine serum albumin; AgNPs, silver nanoparticles; ICG, indocyanine green; PEG-BSA-AgNP/ICG, ICG-loaded PEGylated BSA-coated silver nanoparticles; NIR, near infrared; PBS, phosphate buffer saline.

irradiation, the PEG-BSA-AgNP/ICG sample showed little reduction in the main absorption peak (7%), while other samples revealed substantial reduction (free ICG: 50%, and PEG-BSA-ICG mixture: 34%).

Cellular Analyses of the Anti-Cancer Activity of PEG-BSA-AgNP/ICG

The anti-cancer activity of PEG-BSA-AgNP/ICG with and without laser irradiation was assessed on B16F10 cells. The cytotoxicity results are shown in Figure 5. As seen in Figure 5A, the Ag^+ ions and PEG-BSA-AgNP/ICG showed relatively low but similar profiles of concentration-dependent cytotoxicity. The average IC_{50} values for Ag^+ ions and PEG-BSA-AgNP/ICG were 132 (± 29) and 97 (± 23) μM, respectively. However, as shown in Figure 5B, when the PEG-BSA-AgNP/ICG-treated cells (at 30 μM as Ag, and 20 μg/mL as ICG) were irradiated with laser for 20 min, significantly higher cytotoxic effects were observed ($P < 0.05$, 1-way ANOVA with post hoc analysis of Tukey's multiple comparison test). With increasing cell solution temperature from 40, 45 to 50°C (at laser outputs of 1.1, 1.3, 1.5 W, respectively), higher cytotoxicity was observed (average cell viability: 45%, 11%, 6%, respectively). However, in the absence of PEG-BSA-AgNP/ICG, even with laser irradiation to the cells at 1.5 W, the temperature rise was limited to less than 40°C and little cytotoxicity was observed from the cells.

Pharmacokinetics (PK)

The plasma concentration-vs-time profiles of BSA-AgNP/ICG and PEG-BSA-AgNP/ICG after intravenous administration to ICR mice are shown in Figure 6. Both the PK profiles of BSA-AgNP/ICG and PEG-BSA-AgNP/ICG fitted well with the 1-compartment model. The plasma half-lives ($t_{1/2}$) of BSA-AgNP/ICG and PEG-BSA-AgNP/ICG were 50 min and 112 min, respectively. Compared with the reported plasma half-life of ICG (3–4 min), these results indicated that the encapsulation of ICG in PEGylated BSA silver nanoparticles could not only improve the photostability of ICG but also markedly prolong the blood circulation time.[17]

Biodistribution

The biodistribution profiles of PEG-BSA-AgNP/ICG are summarized in Figure 7. After 4 h post-administration, the PEG-BSA-AgNP/ICG was mainly observed in the liver (Figure 7A) but could be also found in the kidney, lung, and

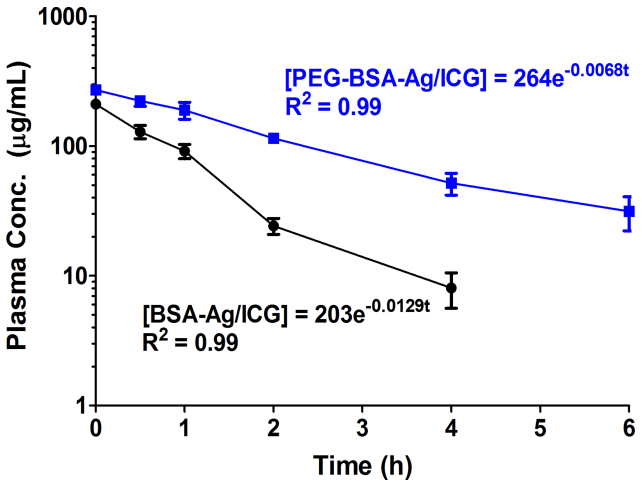

Figure 6 Pharmacokinetic profiles of PEG-BSA-AgNP/ICG. ICR mice (N = 5) were administered with either BSA-Ag/ICG or PEG-BSA-Ag/ICG via tail vein injection at doses of 12 mg/kg as ICG. After then, blood was collected at pre-determined time points (0, 0.5, 1, 2, 4, and 6 h post-administration), and the plasma concentrations of ICG were quantified by measurement of the absorbance at 790 nm.
Abbreviations: PEG, polyethylene glycol; BSA, bovine serum albumin; AgNPs, silver nanoparticles; ICG, indocyanine green; PEG-BSA-AgNP/ICG, ICG-loaded PEGylated BSA-coated silver nanoparticles; NIR, near infrared; PTT, photothermal therapy; ICR, Institute of Cancer Research.

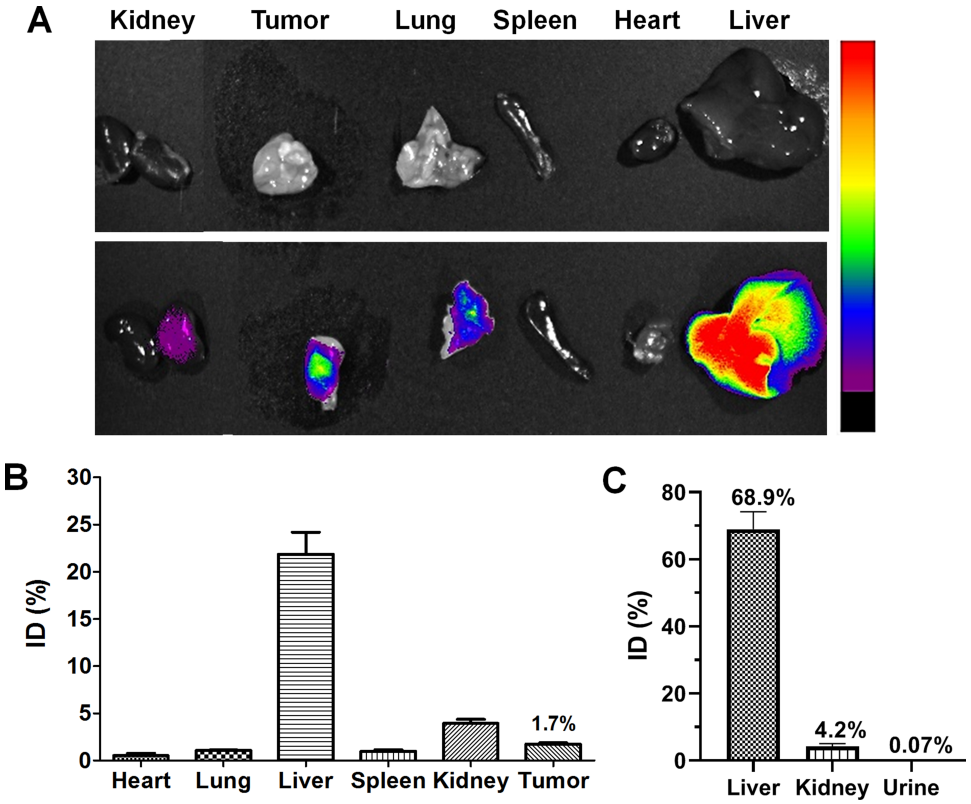

Figure 7 Biodistribution of PEG-BSA-AgNP/ICG in B16F10 in s.c. syngeneic tumor-bearing nude mice. (**A**) When the average tumor size reached 300 mm^3, B16F10 s.c. syngeneic tumor-bearing mice were administered with PEG-BSA-AgNP/ICG (12 mg/kg as ICG) via tail vein injection. At 4 h post-administration, the mice were euthanized and the major organs (kidney, tumor, lung, spleen, heart, and liver) were harvested. The fluorescent images of the mice organs were acquired using FOBI Fluorescence In Vivo Imaging System (NeoScience Co., Ltd., Republic of Korea) (**B**) The ICG contents in the tissues were quantified by measuring the absorbance at 790 nm after the homogenization of the tissues. (**C**) Distribution profiles of silver in liver, kidney and urine at 12 h-post administration of PEG-BSA-AgNP/ICG. **Abbreviations:** PEG, polyethylene glycol; BSA, bovine serum albumin; AgNPs, silver nanoparticles; ICG, indocyanine green; PEG-BSA-AgNP/ICG, ICG-loaded PEGylated BSA-coated silver nanoparticles; NIR, near infrared; PTT, photothermal therapy.

tumor. The quantitative analysis data of the tissue samples were in good accordance with the NIR images (Figure 7B). The tumor accumulation content of PEG-BSA-AgNP/ICG was 1.7% of the injected dose (ID). When the silver contents were measured in the liver, kidney, and urine samples collected at 12 h post-administration (up to 12 h for the urine samples), silver was mostly found from the liver (avg. 68.9% of ID), and a little portion was found in the kidney (4.2% of ID) (Figure 7C). In the urine, only a trace amount (0.07% of ID) was observed (Figure 7C). Despite the high accumulation of the silver in the liver, the liver function analyses data (AST & ALT levels) showed little signs of toxicity. The AST and ALT concentrations of the control mice were 93.5 and 34.0 U/L, respectively, while, for the PEG-BSA-AgNP/ICG-treated mice, they were 106.3 and 38.8 U/L, respectively. These data suggested that the majority of the administered PEG-BSA-AgNP/ICG were safely cleared by the Kupffer cells in the liver.

In vivo Evaluation of the Photothermal Effects of PEG-BSA-AgNP/ICG

At 4 h post-administration of PEG-BSA-AgNP/ICG by tail vein injection, the s.c. tumor site was irradiated with laser for 20 min, and the tumor surface temperature was monitored by IR thermal imaging (Figure 8). The results showed that with greater laser power, higher tumor surface temperature was achieved (38.9°C at 0.5 W – 49.6°C at 0.95 W) (Table 1). Based on the results, 0.9 W of laser output was chosen for the efficacy study.

Efficacy Study in S.c. B16F10 Syngeneic Mice Model

The in vivo anti-cancer activity of PEG-BSA-AgNP/ICG was evaluated in s.c. B16F10 syngeneic mice model. The tumor growth profiles and the bodyweight changes of the mice during the study are shown in Figure 9A and B,

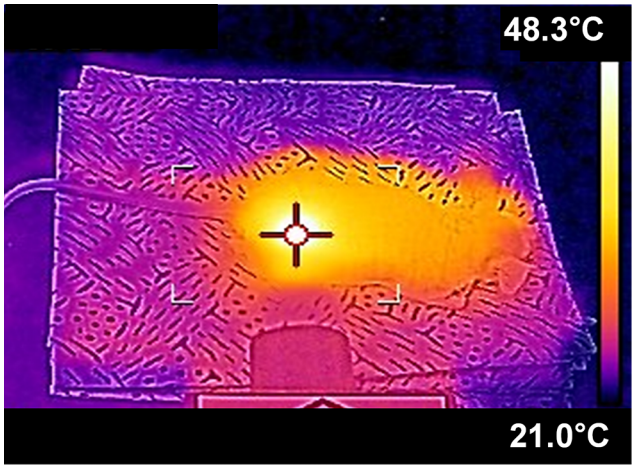

Figure 8 In vivo evaluation of the photothermal activity of PEG-BSA-AgNP/ICG in B16F10 s.c. syngeneic tumor mouse model. When the average tumor size reached 300 mm^3, B16F10 tumor-bearing nude mice (N = 5) were administered with PEG-BSA-AgNP/ICG (12 mg/kg as ICG) via tail vein. At 4 h post-administration, the mice were anesthetized with ketamine/xylazine mixture, and then the tumors were irradiated for 20 min with a diode laser (λ = 885 nm) at varying laser output (0.5–0.95 (W). The highest temperature of the tumor surface was monitored using an infrared camera (E5, FLIR Systems).

Abbreviations: PEG, polyethylene glycol; BSA, bovine serum albumin; AgNPs, silver nanoparticles; ICG, indocyanine green; PEG-BSA-AgNP/ICG, ICG-loaded PEGylated BSA-coated silver nanoparticles; NIR, near infrared; PTT, photothermal therapy.

respectively. As seen from Figure 9A, the tumor sizes of the control group, PBS-treated group with laser irradiation (PBS+PTT) and PEG-BSA-AgNP/ICG-treated group all increased exponentially without any sign of reduction. In a sharp contrast, the tumor sizes of the PEG-BSA-AgNP /ICG-treated mice with laser irradiation (PEG-BSA-AgNP /ICG+PTT) were significantly reduced and most of the tumors were nearly disappeared at the next day of treatment ($P < 0.05$, 1-way ANOVA with post hoc analysis of Tukey's multiple comparison test). For only one mouse of the PEG-BSA-AgNP/ICG+PTT group, the tumor has re-grown at the rim of the original tumor site that may have not received sufficient laser irradiation. At the end of the study (on Day 11), the average tumor sizes were 1014, 903, 896, and 8 mm^3 for PBS control, PBS+PTT, PEG-BSA-AgNP/ICG, and PEG-BSA-AgNP/ICG+PTT, respectively. Regarding the bodyweight (Figure 9B), none of the 4 groups showed a loss during the study. On Day 11, the average increase of bodyweights was 14.9, 18.7, 16.7, and 8.5% for PBS control, PBS+PTT, PEG-BSA-AgNP/ICG, and PEG-BSA-AgNP/ICG+PTT, respectively.

Table 1 Tumor Temperature Monitored for B16F10 S.c. Syngeneic Tumor Mouse Models at 4h Post-Administration of PEG-BSA-AgNP/ICG Using an Infrared Camera (E5, FLIR Systems) with Varied Laser Outputs

Laser Output (W)	Tumor Temperature (°C)
0.95	49.6 ± 4.2
0.9	48.3 ± 3.2
0.8	46.1 ± 3.0
0.7	43.7 ± 2.5
0.6	41.7 ± 2.2
0.5	38.9 ± 2.0

Histological Analysis

After termination of the efficacy study, the tested mice were sacrificed and, histopathological analyses were carried out for their major organs (eg, tumor, kidney, liver, lung, spleen, and heart). The images of the tumor sections are shown in Figure 9B and the tissue sections of other major organs are shown in Figure 10. As seen in Figure 9B, compared with the PBS control group, a marked decrease in the number of tumor cells was observed specifically from the tissue sections of the PEG-BSA-AgNP/ICG+PTT group. However, there was no apparent toxicity observed from all the other major organs (Figure 10).

Discussion

ICG possesses the property of a photosensitizer, which is the ability to convert light to heat.[15] Due to this photothermal activity, it has widely been adopted in researches of developing photothermal therapy (PTT) for the treatment of cancer.[18–20] However, despite its great applicability, the success of effective ICG-based PTT relies heavily on the successful stabilization of the ICG. This is because the ICG suffers from poor photo and plasma stability.[16,17] To address these obstacles, in this research, we developed PEGylated BSA-silver nanoparticles with high loadings of ICG (PEG-BSA-AgNP/ICG).

The PEG-BSA-AgNP/ICG was prepared in 2-steps. At first, the BSA-AgNP/ICG was synthesized by 1-pot chemistry reducing the Ag^+ in the presence of BSA and ICG. Next, the BSA-AgNP/ICG was PEGylated using the NHS chemistry. The physical characterization results for the prepared PEG-BSA-AgNP/ICG by TEM, DLS, UV-VIS spectroscopy and FT-IR proved successful preparation of the nanoparticles (Figures 2 and 3). The PEG-BSA-AgNP /ICG showed high loading of ICG (4.8% loading content against BSA) and excellent size stability for 5 days at storage condition (4°C) (Figure 2C).

The as-prepared PEG-BSA-AgNP/ICG showed superior photostability in vitro to the free ICG. When ICG in the free form was irradiated with a laser, the temperatures of the free ICG solutions decreased to the control baseline level shortly

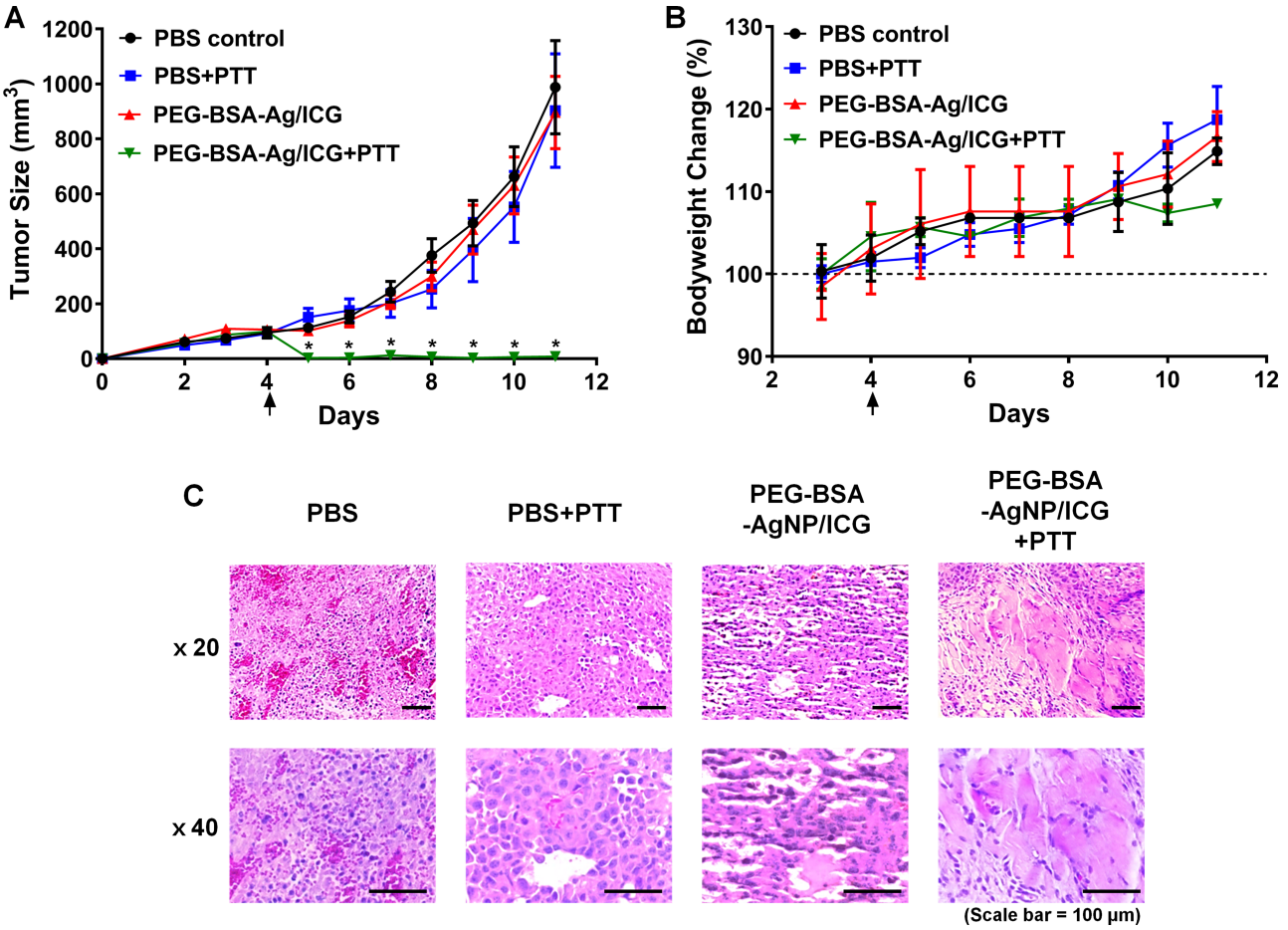

Figure 9 In vivo evaluation of the therapeutic efficacy of PEG-BSA-AgNP/ICG-based photothermal therapy using B16F10 s.c. syngeneic tumor mouse model. (**A**) Tumor growth profiles. When the average tumor size reached 100 mm^3 (at day 4; 4 days after tumor implantation), B16F10 s.c. xenograft tumor mice were randomly divided into 4 groups: 1) PBS, 2) PBS+PTT, 3) PEG-BSA-AgNP/ICG, and 4) PEG-BSA-AgNP/ICG+PTT. The mice were treated once at day 4 and administered with the samples via tail vein injection. Specifically, for groups 2 and 4, at 4 h post-administration, laser was locally irradiated at the tumor site at 0.9W output for 20 min. On day 11 when the average tumor size of PBS-control mice reached 1000 mm^3, the study was terminated. (**B**) Bodyweight changes of the mice. The mice in all groups gained weight during the study and there were no significant differences among the average bodyweights of the groups. The statistically significant difference in the body weight changes among the groups was compared by 1-way ANOVA and post hoc Tukey's multiple comparison test. *$P < 0.05$. (**C**) Representative histological images of the tumor sections. Compared with the tissue sections in other groups, a marked loss of cells was observed from the PEG-BSA-AgNP/ICG-treated mouse tumor.

Abbreviations: PEG, polyethylene glycol; BSA, bovine serum albumin; AgNPs, silver nanoparticles; ICG, indocyanine green; PEG-BSA-AgNP/ICG, ICG-loaded PEGylated BSA-coated silver nanoparticles; UV-VIS, ultraviolet-visible; NIR, near infrared; PBS, phosphate buffer saline.

after reaching the maximum at about 4 min of post-irradiation (Figure 4A). These results indicated that the free ICG was rapidly decomposed by absorbing light. In a sharp contrast, after the temperature of the PEG-BSA-AgNP/ICG solution rose, the highest temperature was maintained through the end of laser irradiation (Figure 4B). Moreover, although the maximum temperature reached by the PEG-BSA-AgNP/ICG was slightly lower than the free ICG and the PEG-BSA-ICG mixture, with laser irradiation of the PEG-BSA-AgNP/ICG solution with light "on" and "off" mode, nearly identical temperature profiles were observed throughout the 3 cycles, while the maximum temperatures of the free ICG solution and the PEG-BSA-ICG were markedly decreased after each cycle (Figure 4C). Collectively, these results indicated that the nanoparticle-loaded ICG could be well protected from light-induced degradation.

From the cellular studies, it was shown that laser-induced heating of PEG-BSA-AgNP/ICG-treated cells above 45°C could induce significantly augmented cytotoxicity (Figure 5B). However, even at the available maximum laser power (1.5 W), the temperature of cells treated with only PBS did not rise above 45°C and showed little cytotoxicity. These results suggested the possibility of selective and effective killing of tumor cells with the PEG-BSA-AgNP/ICG treatment combined with PTT.

Encouraged by the in vitro characterization results, the PEG-BSA-AgNP/ICG was also evaluated in animal studies. First, plasma stability was assessed in vivo. It is well

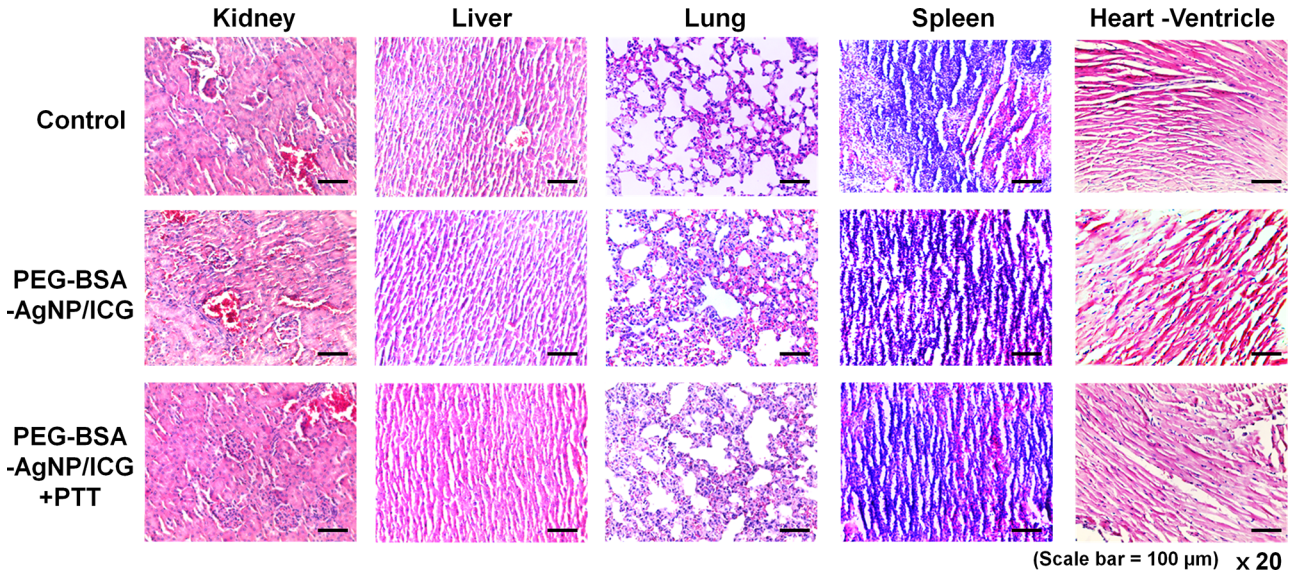

Figure 10 Histological analysis of the nontumorous major organs. After the efficacy study was terminated, the mice were sacrificed and the major organs (kidney, liver, lung, spleen, and heart) were harvested. The paraffin-embedded tissue sections stained with hematoxylin and eosin (H&E) showed no obvious signs of toxicity in organs of all the mice.
Abbreviations: PEG, polyethylene glycol; BSA, bovine serum albumin; AgNPs, silver nanoparticles; ICG, indocyanine green; PEG-BSA-AgNP/ICG, ICG-loaded PEGylated BSA-coated silver nanoparticles; NIR, near infrared; PTT, photothermal therapy.

known that the ICG as a free form possesses very short plasma half-life (3–4 min) and becomes exclusively uptaken by the liver.[17] This could severely halt the tumor accumulation of the ICG after systemic administration and inevitably lead to poor PTT effects. Being an endogenous plasma protein, albumin has a long plasma half-life (approximately 19 days for humans).[32] It is potentially non-toxic and non-immunogenic.[32] Due to these properties, albumin has been widely adopted in many researches as a biomaterial for drug carriers.[33–35] The bioinspired BSA nanoparticles generally possessed favorable characteristics, such as great biocompatibility, biodegradability, prolonged plasma residence, and enhanced tumor distribution.[36,37] Moreover, it has previously been reported that the albumin could even induce selective and higher tumor uptake via interaction with albondin or SPARC (Secreted Protein, Acidic and Rich in Cysteine) overexpressed in cancer cells.[38] In this research, our PK studies demonstrated that, compared to the free ICG, the BSA-silver nanoparticles-loaded ICG could reside in the bloodstream for a significantly longer time (plasma half-life: 50 min). Moreover, the PEG-BSA-AgNP/ICG exhibited an even longer plasma half-life of 112 min than the BSA-AgNP/ICG (Figure 6). This could be explained by the effects of PEG limiting the interaction among the nanoparticles and opsonins, allowing slower clearance through the reticuloendothelial system (RES).[39] Overall, these results evidenced the utility of the bioinspired PEGylated BSA nanoparticles for enhancing the plasma stability of the ICG. Importantly, this prolonged plasma stability led to significant accumulation (1.7% ID/g tissue) of the ICG in the tumor (Figure 7). With the help of improved plasma stability by loading of ICG to the PEGylated BSA silver nanoparticles, over 45°C of tumor surface temperature necessary for the PTT could be achieved by laser irradiation (at higher than 0.8 W of laser output) (Figure 8).

The in vivo efficacy study results in B16F10 s.c. nude mice model confirmed the anti-cancer effects of PEG-BSA -AgNP/ICG. Compared with the control groups, only the treatment group (PEG-BSA-AgNP/ICG+PTT) showed significant inhibition in tumor growth. The histological data also confirmed a marked reduction of cell density only from the tumors of the PEG-BSA-AgNP/ICG+PTT group (Figure 9C). However, with the given dose of 12 mg/kg as ICG, the silver nanoparticle itself did not provide any therapeutic effects as evidenced by the efficacy study results from the PEG-BSA-AgNP/ICG group. Also, the PBS-PTT group showed no significant reduction in the tumor size. This may be explained by the insufficient temperature (38.8°C) to achieve hyperthermia, as it has previously been reported that the tumor temperature should be over 43°C for at least several minutes to achieve hyperthermia-induced cell apoptosis.[40] Apart from the remarkable effects in reducing the tumor size, it was noteworthy that, throughout all the mice tested, systemic toxicity was not observed based on their bodyweight

change profiles (no loss in any group) and the histological analysis data (Figures 9B and 10).

In the PEG-BSA-AgNP/ICG, silver served as the core material of the nanoparticles. It provided a simple and effective way to prepare the ICG-loaded BSA nanoparticles by a 1-step reduction reaction available at low temperatures. Without the silver, the BSA itself could not form an ICG-loaded nanoparticulate system. Despite the usefulness of the silver, the potential toxicity concerns should not be overtaken. The BSA and PEG coatings may be able to prevent the leaching out of soluble silvers to some extent, but, released silvers accumulated in the body could pose potential toxicity concerns.[41] Especially when the silver becomes oxidized to the silver ions, they could induce cell death by generating reactive oxygen species.[42] According to Zhao et al, the surface coating and nanoparticle size could significantly affect the toxicity level of the silver nanoparticles.[43] Therefore, an extensive toxicity evaluation along with further modification studies would be necessary. Overall, in this research, we demonstrated that the PEG-BSA-AgNP/ICG could provide both great photo and plasma stability for the ICG. The long-circulating PEG-BSA-AgNP/ICG could be accumulated in the tumor tissue to a significant level without causing toxicity, and thus sufficient tumor temperature could be achieved in vivo after laser irradiation. Finally, the efficacy studies showed that PEG-BSA-AgNP/ICG-based PTT may be a feasible and effective mode of therapy for the treatment of cancer.

Conclusion

PEG-BSA-AgNP/ICG was successfully prepared and its applicability for PTT was characterized in vitro and in vivo. The major advantages of PEG-BSA-AgNP/ICG lie in the excellent biocompatibility, ease-of-synthesis, minimal quenching (by carrying out the overall synthesis at low temperature), great stability and high loading of ICG. More importantly, it could provide great stability against both light-induced degradation and rapid hepatic clearance. Therefore, the PEG-BSA-AgNP/ICG enabled significant tumor accumulation of the ICG and, with a combination of local irradiation of laser at the tumor site, led to marked tumor growth inhibition. Taken together, our findings from this research demonstrated that the PEG-BSA-AgNP could serve as an effective carrier for the delivery of ICG to the tumor, and the PEG-BSA-AgNP/ICG may be a promising PTT agent for the treatment of cancer.

Funding

This work was financially supported by grants from Basic Science Research Program through the National Research Foundation of Korea (NRF) funded by the Ministry of Education, Science and Technology (NRF- 2018R1D1 A1A02047809 and 2018R1D1A1B07048818).

Disclosure

The authors report no conflicts of interest in this work. The abstract of this paper was presented at the 2019 AAPS Conference as a poster presentation with interim findings: https://www.eventscribe.com/2019/PharmSci360/fsPopup.asp?efp=SUlFUEhHSFQ4MDkx&PosterID=234690&rnd=0.4860628&mode=posterinfo.

References

1. Bao Z, Liu X, Liu Y, et al. Near-infrared light-responsive inorganic nanomaterials for photothermal therapy. *Asian J Pharm Sci*. 2016;11:349–364. doi:10.1016/j.ajps.2015.11.123
2. Fang J, Chen YC. Nanomaterials for photohyperthermia: a review. *Curr Pharm Des*. 2013;19:6622–6634. doi:10.2174/1381612811319370006
3. Nguyen HT, Tran TTP, Jin SG, et al. Combined hyperthermia and chemotherapy as a synergistic anticancer treatment. *J Pharm Investig*. 2019;49:519–526. doi:10.1007/s40005-019-00431-5
4. Lepock JR. Role of nuclear protein denaturation and aggregation in thermal radiosensitization. *Int J Hyperthermia*. 2004;20:115–130. doi:10.1080/02656730310001637334
5. Lepock JR. Cellular effects of hyperthermia: relevance to the minimum dose for thermal damage. *Int J Hyperthermia*. 2003;19:252–266. doi:10.1080/0265673031000065042
6. Zhang W, Guo Z, Huang D, et al. Synergistic effect of chemo-photothermal therapy using PEGylated graphene oxide. *Biomaterials*. 2011;32:8555–8561. doi:10.1016/j.biomaterials.2011.07.071
7. Xu S, Zhu X, Zhang C, et al. Oxygen and Pt(II) self-generating conjugate for synergistic photo-chemo therapy of hypoxic tumor. *Nat Commun*. 2018;9:2053. doi:10.1038/s41467-018-04318-1
8. Luo M, Cheng W, Zeng X, et al. Folic acid-functionalized black phosphorus quantum dots for targeted chemo-photothermal combination cancer therapy. *Pharmaceutics*. 2019;11:242. doi:10.3390/pharmaceutics11050242
9. Kim J, Kim J, Jeong C, et al. Synergistic nanomedicine by combined gene and photothermal therapy. *Adv Drug Deliv Rev*. 2016;98:99–112. doi:10.1016/j.addr.2015.12.018
10. Chen YW, Su YL, Hu SH, et al. Functionalized graphene nanocomposites for enhancing photothermal therapy in tumor treatment. *Adv Drug Deliv Rev*. 2016;105:190–204. doi:10.1016/j.addr.2016.05.022
11. Wei W, Zhang X, Zhang S, et al. Biocompatible and bioactive engineered nanomaterials for targeted tumor photothermal therapy: A review. *Mater Sci Eng C*. 2019;104:109891. doi:10.1016/j.msec.2019.109891
12. Doughty ACV, Hoover AR, Layton E, et al. Nanomaterial applications in photothermal therapy for cancer. *Materials*. 2019;12:779. doi:10.3390/ma12050779
13. Polom K, Murawa D, Rho YS, et al. Current trends and emerging future of indocyanine green usage in surgery and oncology: a literature review. *Cancer*. 2011;117:4812–4822. doi:10.1002/cncr.26087

14. Alander JT, Kaartinen I, Laakso A, et al. A review of indocyanine green fluorescent imaging in surgery. *Int J Biomed Imaging*. 2012;2012:940585. doi:10.1155/2012/940585
15. Sheng Z, Hu D, Xue M, et al. Indocyanine green nanoparticles for theranostic applications. *Nano-Micro Lett*. 2013;5:145–150. doi:10.1007/BF03353743
16. Engel E, Schraml R, Maisch T, et al. Light-induced decomposition of indocyanine green. *Invest Ophthalmol Vis Sci*. 2008;49:1777–1783. doi:10.1167/iovs.07-0911
17. Desmettre T, Devoisselle JM, Mordon S. Fluorescence properties and metabolic features of indocyanine green (ICG) as related to angiography. *Surv Ophthalmol*. 2000;45:15–27. doi:10.1016/S0039-6257(00)00123-5
18. Miao W, Shim G, Kim G, et al. Image-guided synergistic photothermal therapy using photoresponsive imaging agent-loaded graphene-based nanosheets. *J Control Release*. 2015;211:28–36. doi:10.1016/j.jconrel.2015.05.280
19. Lv R, Wang D, Xiao L, et al. Stable ICG-loaded upconversion nanoparticles: silica core/shell theranostic nanoplatform for dual-modal upconversion and photoacoustic imaging together with photothermal therapy. *Sci Rep*. 2017;7:15753. doi:10.1038/s41598-017-16016-x
20. Niu C, Xu Y, An S, et al. Near-infrared induced phase-shifted ICG/Fe3O4 loaded PLGA nanoparticles for photothermal tumor ablation. *Sci Rep*. 2017;7:5490. doi:10.1038/s41598-017-06122-1
21. Wu B, Fu J, Zhou Y, et al. Metal-organic framework-based chemo-photothermal combinational system for precise, rapid, and efficient antibacterial therapeutics. *Pharmaceutics*. 2019;11:463. doi:10.3390/pharmaceutics11090463
22. Azizi M, Ghourchian H, Yazdian F, et al. Anti-cancerous effect of albumin coated silver nanoparticles on MDA-MB 231 human breast cancer cell line. *Sci Rep*. 2017;7:5178. doi:10.1038/s41598-017-05461-3
23. Ding J, Chen G, Chen G, et al. One-pot synthesis of epirubicin-capped silver nanoparticles and their anticancer activity against hep G2 cells. *Pharmaceutics*. 2019;11:123. doi:10.3390/pharmaceutics11030123
24. De Matteis V, Cascione M, Toma CC, et al. Silver nanoparticles: synthetic routes, in vitro toxicity and theranostic applications for cancer disease. *Nanomaterials*. 2018;8:319. doi:10.3390/nano8050319
25. Mirhadi E, Nassirli H, Malaekeh-Nikouei B. An updated review on therapeutic effects of nanoparticle-based formulations of saffron components (safranal, crocin, and crocetin). *J Pharm Investig*. 2020;50:47–58. doi:10.1007/s40005-019-00435-1
26. Kurfurst MM. Detection and molecular weight determination of polyethylene glycol-modified hirudin by staining after sodium dodecyl sulfate-polyacrylamide gel electrophoresis. *Anal Biochem*. 1992;200:244–248. doi:10.1016/0003-2697(92)90460-O
27. Maharjan P, Jin M, Kim D, et al. Evaluation of epithelial transport and oxidative stress protection of nanoengineered curcumin derivative-cyclodextrin formulation for ocular delivery. *Arch Pharm Res*. 2019;42:909–925. doi:10.1007/s12272-019-01154-9
28. Patakfalvi R, Virányi Z, Dékány I. Kinetics of silver nanoparticle growth in aqueous polymer solutions. *Colloid Polym Sci*. 2004;283:299–305. doi:10.1007/s00396-004-1138-8
29. Gerega A, Zolek N, Soltysinski T, et al. Wavelength-resolved measurements of fluorescence lifetime of indocyanine green. *J Biomed Opt*. 2011;16:067010. doi:10.1117/1.3593386
30. Huang H, Yang DP, Liu M, et al. pH-sensitive Au-BSA-DOX-FA nanocomposites for combined CT imaging and targeted drug delivery. *Int J Nanomed*. 2017;12:2829–2843. doi:10.2147/IJN.S128270
31. Zhang J, Shin MC, David AE, et al. Long-circulating heparin-functionalized magnetic nanoparticles for potential application as a protein drug delivery platform. *Mol Pharm*. 2013;10:3892–3902. doi:10.1021/mp400360q
32. Caraceni P, Tufoni M, Bonavita ME. Clinical use of albumin. *Blood Transfus*. 2013;11:s18s25. doi:10.2450/2013.005s
33. Mariam J, Sivakami S, Dongre PM. Albumin corona on nanoparticles - a strategic approach in drug delivery. *Drug Deliv*. 2016;23:2668–2676. doi:10.3109/10717544.2015.1048488
34. Karimi M, Bahrami S, Ravari SB, et al. Albumin nanostructures as advanced drug delivery systems. *Expert Opin Drug Deliv*. 2016;13:1609–1623. doi:10.1080/17425247.2016.1193149
35. Lin HC, Chuang CH, Cheng MH, et al. High potency of SN-38-loaded bovine serum albumin nanoparticles against triple-negative breast cancer. *Pharmaceutics*. 2019;11:569. doi:10.3390/pharmaceutics11110569
36. Kim D, Maharjan P, Jin M, et al. Potential albumin-based antioxidant nanoformulations for ocular protection against oxidative stress. *Pharmaceutics*. 2019;11:297. doi:10.3390/pharmaceutics11070297
37. Kim Y-C, Min KA, Jang D-J, et al. Practical approaches on the long-acting injections. *J Pharm Investig*. 2020;50:147–157. doi:10.1007/s40005-019-00452-0
38. Park CR, Jo JH, Song MG, et al. Secreted protein acidic and rich in cysteine mediates active targeting of human serum albumin in U87MG xenograft mouse models. *Theranostics*. 2019;9:7447–7457. doi:10.7150/thno.34883
39. Mozar FS, Chowdhury EH. PEGylation of carbonate apatite nanoparticles prevents opsonin binding and enhances tumor accumulation of gemcitabine. *J Pharm Sci*. 2018;107:2497–2508. doi:10.1016/j.xphs.2018.05.020
40. Shah BP, Pasquale N, De G, et al. Core-shell nanoparticle-based peptide therapeutics and combined hyperthermia for enhanced cancer cell apoptosis. *ACS Nano*. 2014;8:9379–9387. doi:10.1021/nn503431x
41. Degliangeli F, Kshirsagar P, Brunetti V, et al. Absolute and direct microRNA quantification using DNA–gold nanoparticle probes. *J Am Chem Soc*. 2014;136:2264–2267. doi:10.1021/ja412152x
42. De Matteis V, Malvindi MA, Galeone A, et al. Negligible particle-specific toxicity mechanism of silver nanoparticles: the role of Ag+ ion release in the cytosol. *Nanomedicine*. 2015;11:731–739. doi:10.1016/j.nano.2014.11.002
43. Zhao C-M, Wang W-X. Importance of surface coatings and soluble silver in silver nanoparticles toxicity to Daphnia magna. *Nanotoxicology*. 2012;6:361–370. doi:10.3109/17435390.2011.579632